Rotational dynamics of entangled polymers

J-C. Walter[1,2], M. Laleman[3], M. Baiesi[4,5], and E. Carlon[3]

[1] Laboratoire Charles Coulomb UMR 5221, CNRS & Université Montpellier 2 , F-34095, Montpellier, France
[2] Laboratoire de Microbiologie et Génétique Moléculaire UMR5100, CNRS & Université Paul Sabatier Toulouse 3, F-31000 Toulouse, France
[3] Institute for Theoretical Physics, KU Leuven, Celestijnenlaan 200D, B-3001 Leuven, Belgium
[4] Department of Physics and Astronomy, University of Padua, Via Marzolo 8, I-35131 Padova, Italy
[5] INFN, Sezione di Padova, Via Marzolo 8, I-35131 Padova, Italy

Abstract. Some recent results on the rotational dynamics of polymers are reviewed and extended. We focus here on the relaxation of a polymer, either flexible or semiflexible, initially wrapped around a rigid rod. We also study the steady polymer rotation generated by a constant torque on the rod. The interplay of frictional and entropic forces leads to a complex dynamical behavior characterized by non-trivial universal exponents. The results are based on extensive simulations of polymers undergoing Rouse dynamics and on an analytical approach using force balance and scaling arguments. The analytical results are in general in good agreement with the simulations, showing how a simplified approach can correctly capture the complex dynamical behavior of rotating polymers.

1 Introduction

Polymers, as every system composed by many units, may display a complex dynamical behavior. Even single polymers can show rich and nontrivial dynamical phases, especially if they are subject to spatial or topological constraints [1,2]. The impossibility to break the local connectivity of the polymeric chains is the key to understand interesting global rearrangements of these macromolecules.

In this paper we discuss the rotational dynamics of polymers, where the polymers are either relaxing from a highly entangled configuration by performing a rotational motion or forced to rotate by an applied torque. We briefly review a series of published results [3–6] and extend our analysis to some new cases not considered so far. There are two main motivations to justify this study. First, the rotational motion is a central instance in polymer dynamics. Our analysis is based on the results of extensive numerical simulations, which are supported by analytical arguments. The comparison between the two approaches can teach us about the validity and possible shortcomings of the approximations used in the analytical calculations. This is a valuable input for other studies of polymer dynamics. Second, it has applications to some interesting biological *in vitro* problems: the DNA double helix melting [7,8],
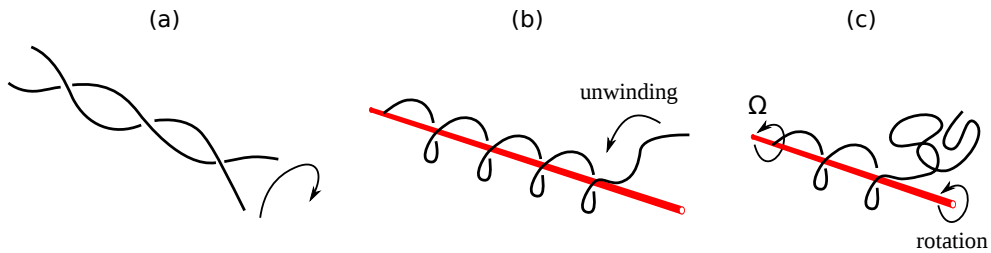
Fig. 1. Examples of rotational dynamics of entangled polymers. (a) The unwinding dynamics of two polymer chains dissociating from each other. (b) The unwinding of a single chain from a rigid rod. (c) The stationary conformation of a polymer attached to a rod rotating with a constant angular velocity Ω.

RNA unwinding during transcription [9,10] and the closure of denaturation bubbles in DNA [11] are some examples (*in vivo*, the relaxation of topological constraints of the DNA is achieved in various ways, often involving molecular motors like chromatin remodellers, polymerases...).

Examples of rotational dynamics are shown in Fig. 1. Consider for instance two polymers wrapped around each other as in a double-stranded DNA helix as sketched in Fig. 1(a). When brought at high temperatures or to specific solvent conditions, DNA hydrogen bonds break [8] and the two strands dissociate from each other. The dissociation must involve some rotational motion necessary to disentangle the two strands, as those of Fig. 1(a). Studies of DNA denaturation dynamics have revealed that the constraint of excluded volume slows down this relaxation [12,13,3,4,14], with time scales that grow as a power-law of the chain length. A simpler system is the unwinding of a single polymer from a rigid rod [5,6], see the sketch in Fig. 1(b). Here, the advantage is the possibility to follow the dynamics by monitoring the winding angle of the last monomer.

The winding angle plays the role of a reaction coordinate. Unfortunately, this quantity cannot be defined for the unwinding of two strands. In the case of unwinding from a rod, the knowledge of the equilibrium statistics of the winding angle [15,16] simplifies considerably the theoretical treatment of single-polymer unwinding dynamics [5,6,10]. Here again excluded volume is the only interaction between rod and polymer. The unwinding dynamics of a polymer from a rod can be viewed as a simple model of the dynamics of a newly synthesized mRNA molecule that is clumped to the DNA it was transcribed from [10]. Indeed, RNA polymerase moves as a train on the three-dimensional railroad represented by a double stranded DNA: in the frame where DNA is steady, the trajectory where the RNA is generated by polymerase is a helix around the DNA backbone. As biological polymers are often stiff, a natural extension of the previous work is the study of the unwinding dynamics of semi-flexible polymers, which is discussed in this paper.

Another setup discussed in this work is shown in Fig. 1(c): here the rod rotates under the influence of a constant applied torque that leads to a constant angular velocity Ω. The polymer is attached to the surface of the rod by a single monomer and is driven to a nonequilibrium steady rotational regime. In this setup the impenetrable rod is fundamental to force the rotation of the flexible polymer, as opposed to the case where a polymer with some torsional rigidity (e.g. double stranded DNA) is set into motion by a torque applied at one end [17–19].
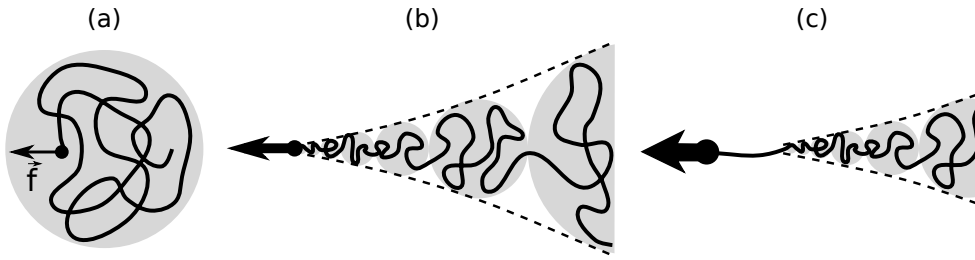
Fig. 2. A polymer pulled from one end by a constant force displays three different dynamical regimes. (a) At weak forces the polymer is not significantly perturbed with respect to the equilibrium conformation. (b) At intermediate forces the polymer assumes the shape of a trumpet. (c) At strong forces a part of the polymer close to the pulled end is fully stretched, while a trumpet developes at the end part.

1.1 Polymers pulled from one end: a brief review

The processes discussed in this paper are in a sense the rotational counterparts of processes that have been studied for quite some time in linearly stretched flexible polymers [20–24] and in semi-flexible polymers [25].

Consider for instance a strong flow stretching a tethered polymer to its full elongation. When the flow is stopped, the polymer recoils back into its equilibrium conformation, starting from its free end: the dynamics of Fig. 1(b) is the rotational equivalent of the recoiling of a stretched polymer. Similarly, for a polymer forced to rotate around a rigid rod at constant angular velocity (Fig. 1(c)), the counterpart is a polymer pulled from one end by a constant force. As we will make use of scaling arguments borrowed from the latter case, we recall briefly the three different dynamical regimes one finds in polymers pulled from one end. In the weak force regime the polymer shape is not perturbed appreciably compared to its equilibrium coiled conformation (Fig. 2(a)). This occurs when $f \lesssim k_B T / R_F$ where k_B is the Boltzmann constant, T the temperature and R_F the equilibrium Flory radius of the polymer. For a flexible polymer with L monomers separated by a distance a one has $R_F = aL^\nu$, where ν is the Flory exponent [26]. In an intermediate force regime, corresponding to $k_B T / R_F \lesssim f \lesssim k_B T / a$, the polymer assumes a "trumpet" shape as illustrated in Fig. 2(b). It can be considered as being composed by a sequence of blobs of size $\xi(x)$, which increases starting from the pulled end (x is the direction along which the force is applied). Finally, in the strong force regime where $f \gtrsim k_B T / a$ the pulled end is followed by a stretched portion of polymer (Fig. 2(c)), which converts into a trumpet shape at some point along the chain. We will show that these concepts enter naturally also in the characterization of rotational or unwinding dynamics.

1.2 Simulated models

In order to test the universality of the results, different on- and off-lattice models were simulated in two and three dimensions. In this paper we focus on simulations of ideal polymers, which are more efficient to implement. A polymer is composed of L links of length a that is set to unity. Thus, in the following L means the length of the polymer in unit of a. In 3D the only excluded volume interactions are between the polymer and the rod whereas in 2D excluded volume interactions are between the polymer and a disk in the plane. In simulations, the rod is chosen large enough to avoid the polymer to cross it during a move. Specifically the following models were simulated: Random Walks (RWs) on square (2D) and on FCC (3D) lattices and the discrete
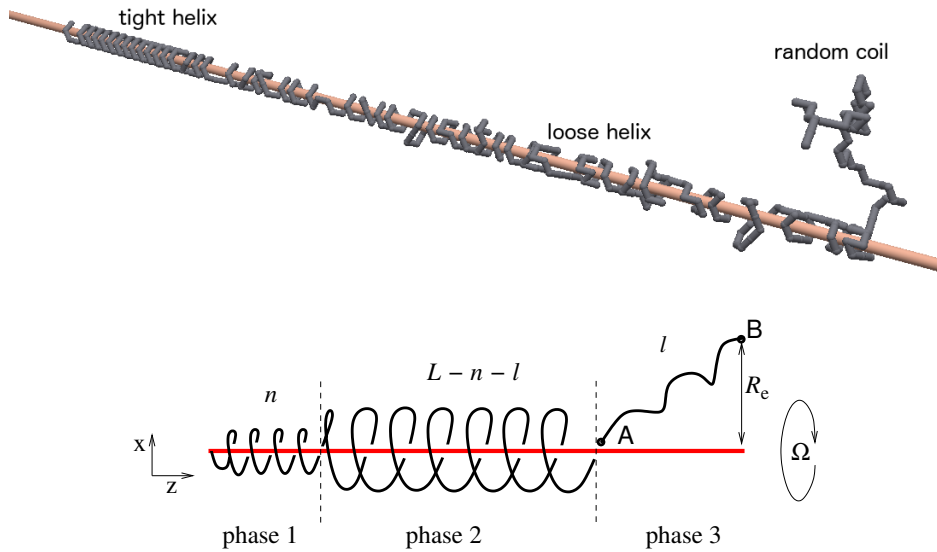
Fig. 3. Top: Snapshot of a simulation of a RW relaxing from an initial conformation tightly wrapped around a rod. The snapshot suggests that the dynamics could be modeled by a three phase model (bottom figure). The three phase are a tight (frozen) helix, a looser helix and an end coil.

worm like chain (WLC) [27] off-lattice in 3D. In the WLC a polymer configuration is characterized by angles α_i (with $1 < i < L$) between two consecutive bonds. Each angle contributes to the bending energy with a term $-\cos \alpha_i$. A configuration at inverse temperature β thus carries a Boltzmann weight $\exp[\beta \sum_i \cos \alpha_i]$ where $\beta \equiv 1/(k_B T)$ is the inverse temperature, T the temperature and k_B the Boltzmann constant. In the following, the inverse temperature β will be expressed in inverse unit of k_B that is set to unity. The WLC has the property to be rigid at the scale of the persistence length l_p that is an increasing function of the temperature. At low temperature, $l_p \sim \beta$, whereas in the high temperature limit $\beta \to 0$ one recovers the freely jointed chain (FJC). The dynamics was implemented using either a kinetic Monte Carlo update, with Metropolis accepting rules, or a Langevin thermostat [28]. Both schemes are implementations of Rouse dynamics [1]. In Monte Carlo simulations the time unit corresponds to L attempted local moves.

2 Relaxation dynamics of a polymer wrapped around a rod

In this section we consider the relaxation dynamics of a polymer initially wrapped around an infinitely long rod. We start from reviewing the predictions of the three phase model for flexible polymers [5,6] and extend the analysis to semiflexible polymers.

Consider a polymer initially tightly wound around a long rod axis, to which it is attached by one end. The free end then starts rotating around the rod until the polymer gets fully unwound so as to maximize its entropy. Snapshots of simulation runs [5,6] suggest that the polymer can be thought of as being composed of three different phases as displayed in Fig. 3: a part of the polymer close to the end monomer attached to the rod is "frozen" as in its initial helical configuration (phase 1); in its central part the polymer is still wrapped around the rod, but more loosely compared to the initial configuration (phase 2); finally there is a terminal region detached from

the rod in a random coil configuration (phase 3). This suggests that a minimal model of the dynamics of the system should include these three phases. To simplify the description, we assume that phase 2 forms a homogeneous helix with a constant pace and that the end coil assumes an equilibrium conformation (this assumption is actually verified in simulations [6]). In the course of time phase 2 and 3 grow at the cost of phase 1. However, ultimately also phase 2 vanishes and only phase 3 remains because random coils are the typical equilibrium configurations (with null winding in average, but fluctuations scaling as the logarithm of the chain length [16]). In this paper we focus mainly on the early stage of the unwinding, when the three phase coexist.

Two phase models have gained some popularity in recent studies of polymer dynamics [29,23,24]. Such models are simple enough, but also quite effective to capture the non-equilibrium dynamics of polymers set into motion, for instance by a force pulling one of their ends or during translocation. As the dynamics involves a mechanism of tension propagation along the polymer backbone, some time is needed before the effect of the perturbation reaches the opposite end of the polymer. In a two phase picture one subdivides the polymer into a moving domain and a domain still at equilibrium, and focuses on the dynamics of the boundary between the two phases. For instance, in a model of polymer translocation, Sakaue [29] identifies a moving phase close to the pore that propagates at the expense of a rest phase located far from the pore. Two phase models have also been used recently in studies of polymers pulled by one end [23,24] and for DNA hairpin dynamics [14]. Interestingly, in our case, a minimal model of the relaxation dynamics of a polymer wrapped around a rod requires three phases rather than two. We are not aware of other types of three phase models in the context of polymer dynamics.

2.1 Theory

We briefly review some of the predictions of the three phase model, without entering in the details. The Appendix provides additional schematic informations about the derivation of the main results. More details can be found in [6]. Let us consider first a fully flexible polymer. Using a force-balance argument [6] one can show that phase 1 shrinks as:

$$L - n \sim \sqrt{t}. \tag{1}$$

The notation is also summarized in Fig. 3: L is the total length of the polymer, while n and l are the lengths of phase 1 and phase 3, respectively. As phase 1 shrinks the fraction of the polymer in phases 2 and 3 rotate in a corkscrew motion around the rod. This is where the excluded volume of the rod-polymer system plays a crucial role: if the polymer could trespass the rod, the initial phase would melt immediately. In reality this does not happen and phase 2 can increase only if phase 3 is also rotating around the rod. The unwinding of phase 2 and 3 is thus the only mechanism that leads to a decrease of the total winding angle. The angular velocity is $\Omega \sim 1/\sqrt{t}$, as obtained by differentiating Eq. (1) (see Ref.[6] and Appendix). Here Ω decreases in time as during unwinding a growing fraction of the polymer is set into motion, leading to an increase of the friction. A scaling argument (see Ref. [6] and Appendix) yields the following prediction for the growth dynamics of phase 3:

$$l \sim t^{1/(4\nu+2)}, \tag{2}$$

where ν is the Flory exponent ($\nu = 1/2$ for a Gaussian polymer and $\nu \approx 0.59$ for a self-avoiding polymer [1]). Interestingly, the dynamics of the two boundaries (between phase 1 and phase 2 and between phase 2 and phase 3) is characterized by different

exponents (Eqs. (1) and (2), respectively). Also the scaling dynamics of the distance of the free end monomer (point B in Fig. 3) from the rod, denoted by R_e, can be inferred from Eq. (2)

$$R_e \sim l^\nu \sim t^{1/z}\,, \tag{3}$$

where the dynamical exponent is given by $z = 4 + 2/\nu$.

Semiflexible polymer are characterized by an additional length scale, l_p, the persistence length. At lengths $l \ll l_p$ the polymer behaves as a stiff rod. In the initial stages of unwinding, when the phase 3 is still short so that $l \ll l_p$, we expect the following growth law:

$$l \sim t^{1/6}\,. \tag{4}$$

This can be obtained by formally setting $\nu = 1$ in Eq. (2), as expected for a stiff polymer segment. Similarly, one finds from Eq. (4):

$$R_e \sim l \sim t^{1/z}\,, \tag{5}$$

with $z = 6$. These formulas work as long as the phase 3 is formed by a stiff straight segment. We expect a crossover to the flexible case (characterized by Eqs.(2) and (3)) when the length of phase 3 exceeds the persistence length of the polymer, i.e., $l \gtrsim l_p$.

The total winding angle is defined as $\Theta \equiv 2\pi n_{\text{turns}}$, where n_{turns} is the number of turns (assumed to be a continuous variable) that the polymer performs around the rod, starting from the fixed end to the free one. It is convenient to introduce the mean density of winding $\Delta\theta_1$ (for phase 1, the initial total winding angle is thus $\Theta_0 = L\Delta\theta_1$) and $\Delta\theta_2$ (for phase 2). One has:

$$\Theta = n\Delta\theta_1 + (L - l - n)\Delta\theta_2\,, \tag{6}$$

as the coil (of length l) does not contribute to the winding. Combining Eqs. (1), (2) and (6), we get:

$$
\begin{aligned}
\Theta_0 - \Theta &= (L - n)(\Delta\theta_1 - \Delta\theta_2) + l\Delta\theta_2 = At^{1/2} + Bt^{1/\alpha}\,, \\
&= At^{1/2}\left(1 + \frac{B}{A}\frac{1}{t^{1/2 - 1/\alpha}}\right)\,,
\end{aligned} \tag{7}
$$

where $\alpha = 4\nu + 2$ ($\alpha = 6$) in the flexible (semiflexible) case, respectively. Here A and B are positive constants. The prediction is that $\Theta_0 - \Theta$ scales as $\sim \sqrt{t}$, with a slowly decaying correction term originating from the contribution of phase 3.

Note that in a fully analogous way we can define the winding angle for any monomer. We indicate with $\theta(m)$ the local winding angle of the m-th monomer, counted from the monomer fixed at the rod. The total winding angle is then $\Theta = \theta(L)$. The three phase model predicts the following linear piecewise profile for the local winding angle:

$$
\theta(m) = \begin{cases}
m\Delta\theta_1 & \text{if } m \leq n \\
n\Delta\theta_1 + (m - n)\Delta\theta_2 & \text{if } n \leq m \leq L - l \\
n\Delta\theta_1 + (L - l - n)\Delta\theta_2 & \text{if } L - l \leq m \leq L
\end{cases} \tag{8}
$$

2.2 Simulations

Having discussed the predictions of the three-phase model we focus now on results from simulations, which turn out to be in very good agreement with the theory. As we
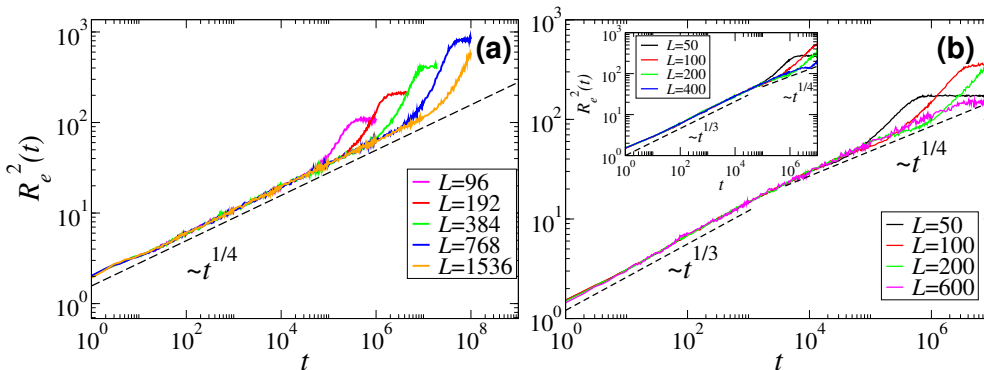
Fig. 4. Log-log plot of the squared end-to-rod distance $R_e^2(t)$ vs. t for polymers of various lengths L. The panel (a) shows result for a flexible polymer model (3D RW on a FCC lattice). The short time regime fits the behavior predicted by Eq. (3) with $z = 8$, i.e. $R_e^2(t) \sim t^{1/4}$. The panel (b) displays the same quantity for the WLC. In the main graph ($\beta = 3$) it shows a crossover between two regimes ($t \approx 2\,000$). A new regime $R_e^2(t) \sim t^{1/3}$, i.e. $z = 6$ in Eq. (5) appears at short times. Inset: The same quantity for the WLC at $\beta = 5$. Note that at lower temperatures the regime scaling as $R_e^2(t) \sim t^{1/3}$ extends to a wider time interval ($t \approx 50\,000$). The persistence length being larger, the condition $l \gtrsim l_p$ occurs later, as expected.

will only show results for ideal polymers, we can set $\nu = 1/2$, which is the Gaussian value. However, the results have also been tested for self-avoiding polymers [6]. We consider first in Fig. 4 a log-log plot of the squared end-to-rod distance R_e^2 vs. time t for different polymer lengths. We show in panel (a) the flexible case with (3D RW on a FCC lattice) and (b) the semiflexible case (WLC at $\beta = 3$). In both cases we observe a power-law behavior at short times. Deviations from this behavior at longer times indicate a different type of relaxation, which is not discussed in this article. In the flexible case (a), the dashed line has a slope $2/z$ with $z = 2/\nu + 4 = 8$, in very good agreement with the prediction of Eq. (3). In the semiflexible case (b) one notices a crossover between two regimes: $R_e^2 \sim t^{2/z}$ with $z = 6$ at short times moving back to the flexible case $z = 2/\nu + 4 = 8$ at longer times ($t \approx 2\,000$), when the random coil becomes long enough. In the inset of Fig. 4(b), the simulations are performed at $\beta = 5$ where the equilibrium persistence length l_p is larger than the main graph. As expected, we notice that the cross-over occurs at a larger time ($t \approx 50\,000$), indicating that the random coil needs to grow larger to enter into the flexible polymer regime.

We continue the analysis of simulation results to test of the validity of Eq. (1). To identify the boundary between phase 1 and phase 2, we consider the local winding angle $\theta(m)$ as a function of the monomer number m. A plot of $\theta(m)$ vs. m for different times is shown in Fig. 5 for (a) a flexible polymer (2D RW of length $L = 512$) and for (b) a semiflexible polymer (WLC of length $L = 400$). At $t = 0$ the polymer is prepared in phase 1 so the local winding angle is $\theta(m) = m\Delta\theta_1$ (dashed lines in both figures). At intermediate times the three phase model predicts that the local winding angle is a piecewise linear function (Eq. (8)). The numerical results for $\theta(m)$ instead do not show sharp boundaries: the average over different simulation runs produces a smooth continuous curve. We note that while in the flexible case the local winding angle decreases monotonically in time, this is not the case for the semiflexible polymer. Starting from the $t = 0$ tight helix configuration (dashed line in Fig. 5(b)) there is a slight increase in $\theta(m)$ in the phase 1, as indicated by the horizontal arrows (three largest times only). This appears to be a small effect though. To determine $n(t)$, the length of the phase 1, we took in the semiflexible case the intersection of the $\theta(m)$ vs. m curve with the line $\theta(m) = m\Delta\theta_1$. In the flexible case we took the value of
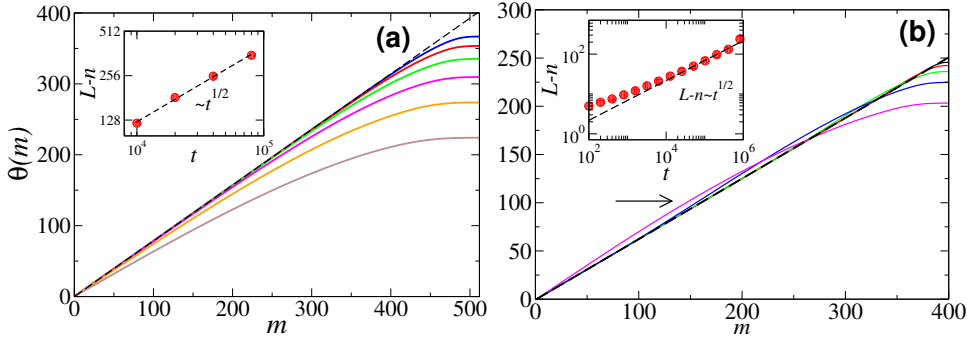
Fig. 5. Plot of local winding angle $\theta(m)$ vs. monomer number m for different times for (a) the flexible case (2D RW of length $L = 512$ on a square lattice, curves for $t = 10^4$ up to $t = 32 \times 10^4$ doubling t) and (b) the WLC at $\beta = 2$ and for a length $L = 400$. From top to bottom, the times run from $t = 100 \times 2^4$ to 100×2^{12}, multiplying t by 4. The horizontal arrows point (for the three largest times only) to the start of the slight increase of $\theta(m)$ in the phase 1, which does not occur in (a). (Insets) Log-log plot of the length $L - n$ of phase 2, vs. t for the (a) flexible and (b) semiflexible case. The dashed lines have slope $1/2$, as predicted from Eq. (1).
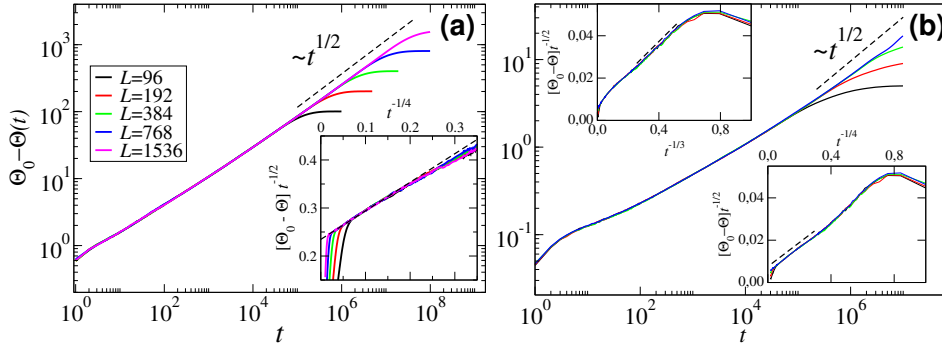

Fig. 6. Amount of unwinding for (a) a flexible polymer (RW on a FCC lattice) and (b) a semiflexible polymer (WLC at $\beta = 5$). Insets: corrections to scaling. In (b) the two insets show that there is a crossover also in the correction to scaling from the exponent $-1/3$ at small time and $-1/4$ at large time.

m from which $\theta(m)$ drops to 95% of the initial $t = 0$ value. In both cases the data follow the expected $\sqrt{t}$ behavior (see insets of Fig. 5). The results are in agreement with Eq. (1).

We focus next on the dynamics of the total winding angle and test the validity of Eq. (7). A log-log plot of $\Theta_0 - \Theta$ as a function of time is shown in Fig. 6. This quantity approaches the $\sqrt{t}$ behavior predicted by Eq. (7), but with strong corrections to the dominant scaling. To investigate the leading corrections to scaling reported in Eq. (7), we plot in the insets $(\Theta_0 - \Theta)/\sqrt{t}$ as a function of $1/t^{1/2 - 1/\alpha}$. According to Eq. (7), this quantity should follow a straight line. This is indeed the case as can be seen in the inset of Fig. 6(a). Note that for the flexible case the correction term is $t^{-1/4}$ (for RW, $\nu = 1/2$) while it is equal to $t^{-1/3}$ for semiflexible polymers. In the insets of Fig. 6(b), we observe the crossover between the term $t^{-1/3}$ at small time and $t^{-1/4}$ at large time, confirming the prediction of our model.

3 Stationary rotating polymer

We focus now on the case of a polymer fixed by one end monomer to a rod to which a constant torque is applied, as sketched in Fig. 1(c). We restrict ourselves to the flexible case. After a transient regime, the polymer enters a stationary nonequilibrium state where it rotates around the rod with a constant angular velocity Ω. Analogous to the case of a polymer pulled by a constant force by one end, we expect that a weak torque would not be able to perturb the polymer significantly from its equilibrium conformation. The relation (17), derived in the Appendix, characterizes the weak torque regime. This inequality can be interpreted as follows: polymers rotating with an angular velocity Ω, but shorter than a critical length

$$L_c = \left(\frac{k_B T}{a \gamma_0 \Omega} \right)^{1/(1+2\nu)}, \tag{9}$$

will rotate around the rod maintaining their random coil shape. Polymers with length $L > L_c$ will instead be partially wrapped around the rod: only the L_c monomers at the free end may form an equilibrated coil. To test the validity of these scaling arguments we analyzed the behavior of the squared end distance from the rod, R_e^2, as a function of Ω. In the weak torque regime the full chain rotates in an equilibrium configuration around the rod, and thus $R_e^2 \sim L^{2\nu}$. In the high torque regime only L_c monomers can be in an equilibrium configuration, hence $R_e^2 \sim L_c^{2\nu} \sim \Omega^{-2\nu/(1+2\nu)}$. The two regimes can be connected by means of a scaling function:

$$R_e^2 = L^{2\nu} g \left(L \Omega^{1/(1+2\nu)} \right) \tag{10}$$

where the natural scaling variable is $x = L\Omega^{1/(1+2\nu)}$. The scaling function in the large Ω limit behaves as $\lim_{x\to\infty} g(x) = x^{-2\nu}$, while it tends to a constant limit for small values of its argument.

We simulate a polymer composed by L beads on a continuum using a Langevin thermostat [28]. Each bead interacts with its neighbors along the polymer via a FENE potential. The interaction with the rod is modeled by a repulsive truncated Lennard-Jones potential with radius $r_{\text{rod}} = 0.75a$. The distance a between beads was normalized to one, just as k_B and the mass of a bead m. The equations of motion were integrated using a time step of $\Delta t = 0.001$. The bath was at a temperature $T = 80$ and the friction coefficient set to $\gamma_0 = 10^3$. The FENE potential had a spring constant of $2.36 \cdot 10^5$ and a maximal extensibility of $1.5a$. In the simulation we apply a constant force F perpendicular to the axis of the rod to one end monomer. This monomer is constrained to move on a radius r_{rod} from the axis of the rod. The applied torque $M = Fr_{\text{rod}}$ induces a constant angular velocity to the polymer which can be obtained by averaging over the velocities of all monomers, once the polymer has reached the stationary regime. Figure 7(a) shows a log-log plot of the squared end-to-rod distance as a function of Ω for polymers of various lengths. The dashed line, in agreement with the data at high Ω, corresponds to a scaling $R_e^2 \sim 1/\sqrt{\Omega}$ which is the behavior predicted from the scaling argument derived above (again we use $\nu = 1/2$, which is the value for a gaussian polymer). In addition appropriately rescaled data collapse in good agreement with the scaling form (10), as shown in the inset of Fig. 7(a).

A rigid body rotating in a viscous medium under the effect of a torque M is characterized by a linear relationship between torque and angular velocity Ω

$$M = \Gamma \Omega, \tag{11}$$

where Γ is the rotational friction. We can estimate Γ for a polymer rotating around the rod for some specific polymer conformations. Let us suppose first that the polymer
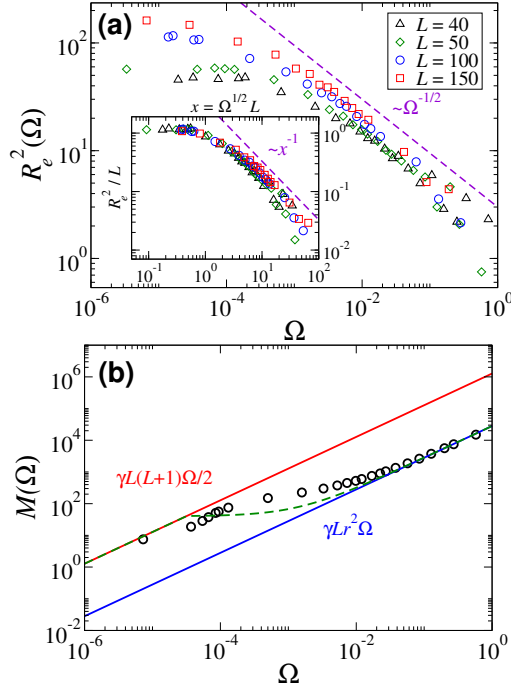
Fig. 7. (a) The end-to-rod distance as a function of the angular velocity for differents sizes. For low angular velocities the polymer rotates in equilibrium configuration around the rod. For higher velocities the two phase model predicts that R_e should scale as $\Omega^{-0.5}$. Inset: rescaling according to Eq. (10). (b) Torque vs. angular velocity, for $L = 50$. Only for low and high angular velocities a linear relation is expected, at intermediate values of Ω a more complicated behavior emerges. The straight lines represent predicted asymptotic scalings, while the dashed line is the scaling from a simple two phase model.

is in an equilibrated coiled conformation, which is what we expect to observe at low Ω's. In equilibrium the l-th monomer is at an average distance $r^2(l) = a^2 l$ from the rod. Assuming that each monomer contributes a term $\gamma_0 r^2(l)$ to the friction we get

$$\Gamma_{\text{coil}} = \sum_{l=1}^{L} \gamma_0 a^2 l = \frac{\gamma_0 a^2}{2} L(L+1). \tag{12}$$

As a second case consider a polymer fully and tightly wrapped around the rod, i.e. as in a helix where each monomer is at a distance r_{rod} from the rod. The rotational friction is equal to

$$\Gamma_{\text{helix}} = \gamma_0 r_{\text{rod}}^2 L. \tag{13}$$

In Fig. 7(b) we show a log-log plot of M vs. Ω as obtained from simulations. The two solid lines are $M = \Gamma_{\text{coil}}\Omega$ and $M = \Gamma_{\text{helix}}\Omega$ from Eqs. (12) and (13) without any fitting parameters. The simulation data interpolate between these two limits: as expected the polymer is coiled at low torques and gets fully wrapped around the rod at high torques. We can get an interpolating formula for Γ in the intermediate regime using a two phase model. We assume that there are two distinct contributions to the friction coming from an end coil of length l and of a wrapped part of length $L - l$ leading to:

$$\Gamma_{\text{tot}}(L, l) = \Gamma_{\text{coil}}(l) + \Gamma_{\text{helix}}(L - l). \tag{14}$$

We use Eq. (9) to estimate l and set $l = \tilde{L}_c = \min(L_c, L)$. In Fig. 7(b) we plot the curve $M = \Gamma_{\mathrm{tot}}(L, \tilde{L}_c)\Omega$, which is shown as a dashed line. Again, there are no fitting parameters in this computation. Note that Γ_{tot} depends on Ω through L_c, see Eq. (9). The analytical calculation reproduces qualitatively the crossover behavior between the two regimes, although there are some systematic deviations. In particular, the analytical computation underestimates the friction. This is because the helical phase is assumed to be tightly wrapped around the rod with all monomers at distance $r(l) = r_{\mathrm{rod}}$ from the rod axis. In reality, the monomers are expected to be more loosely wrapped around the rod, producing a larger friction than the estimate of Eq. (13). Future work will focus on a construction of a better approximation for Γ.

4 Conclusions

In this paper we have reviewed some recent results about the rotational dynamics of a single flexible polymer around a rod [5,6] and extended the analysis to new cases. Two situations have been discussed: the relaxational dynamics of a polymer initially wrapped around a rigid rod and a polymer forced to rotate by a constant applied force. In the former case we have shown how a force-balance argument, relying on a three phase model, allows to derive the universal exponents describing the relaxational dynamics of various quantities as the end-distance from the rod or the winding angle. The results have been extended here to the case of semiflexible polymers which show a crossover between different regimes. In general, a very good agreement between theory and simulations is found. In a polymer rotating under the influence of an applied torque we have analyzed the dependence of the end-distance from the rod on the angular velocity, which matches the predictions from scaling theory. We have shown that there is a non-linear relationship between torque and angular velocity which is due to a conformational transition in the polymer from a coiled to a wrapped state. A two phase model calculation, without any adjustable parameters, reproduces semi-quantitatively the torque vs. angular velocity curves obtained from simulations.

In conclusion, although the models discussed are rather simple, our analysis shows that there is an underlying rich and complex dynamics. The analytical and scaling arguments developed to study these simple systems can guide us towards the understanding of more complex cases of polymer dynamics. The study of polymers disentangling from linear objects is also of interest for a better understanding of some aspects of RNA and DNA dynamics.

Acknowledgements

Appendix

We provide some details about the derivation of the results of Section 2 (see also Ref. [6]). To describe the dynamics of the polymer rotating around the rod we neglect first the contribution of phase 3. The total free energy of the system is given by

$\mathcal{F}(n) = f_1 n + f_2(L - n)$, where f_1 and f_2 are the free energies per unit of polymer length for the phase 1 and 2 respectively. When phase 1 shrinks the phases 2 and 3 rotate in a corkscrew motion; neglecting phase 3, the friction associated with the dynamics comes from phase 2 and scales as the length of this phase $\gamma_2 \sim L - n$. The balance of frictional and entropic forces gives:

$$\gamma_2 \frac{dn}{dt} = -\frac{\partial \mathcal{F}}{\partial n} \tag{15}$$

Using the above forms for γ_2 and $\mathcal{F}$ one can easily integrate the previous differential equation to get the square root growth predicted by Eq. (1). To derive Eq. (2) we use the analogy with a polymer pulled from one end by a constant force f. As discussed in the introduction the weak force regime of Fig. 2(a) is given by

$$f R_F \lesssim k_B T \tag{16}$$

Consider a polymer rotating around an axis with an angular velocity Ω. The average distance from the axis is R_F, so the linear velocity is $v \approx \Omega R_F$ and the frictional force is thus $f \approx \gamma \Omega R_F$. In Rouse dynamics the friction is proportional to the polymer length $\gamma \approx \gamma_0 l$ [1]. Summarizing, the inequality (16) for a rotating polymer becomes:

$$a \gamma_0 \, l^{1+2\nu} \Omega \lesssim k_B T. \tag{17}$$

Hence a polymer of length l rotating around its axis with an angular velocity Ω sufficiently small such that Eq. (17) is satisfied will maintain its equilibrium shape. If Ω is large enough such that Eq. (17) is not fulfilled, then part of the polymer will be wrapped around the rod. For a polymer relaxing from an entangled state around a rod, we need the time evolution of Ω stated in Section 2. Using Eq. (6), and assuming a faster growth for $L - n$ compared to l, we find to leading order in t:

$$\Omega = \frac{d\Theta}{dt} \sim \frac{dn}{dt} \sim \frac{1}{\sqrt{t}} \, , \tag{18}$$

where we have used Eq. (1). Then, one can use the relation (17) in the form of an equality to obtain Eq. (2).

References

1. M. Doi, S.F. Edwards, *The Theory of Polymer Dynamics* (Oxford University Press, New York, 1989)
2. M. Muthukumar, *Polymer Translocation* (CRC Press, 2011)
3. M. Baiesi, G.T. Barkema, E. Carlon, D. Panja, J. Chem. Phys. **133**, 154907 (2010)
4. M. Baiesi, E. Carlon, Markov Proc. Relat. Fields **19**, 569 (2013)
5. J.C. Walter, M. Baiesi, G.T. Barkema, E. Carlon, Phys. Rev. Lett. **110**, 068301 (2013)
6. J.C. Walter, M. Baiesi, E. Carlon, H. Schiessel, Macromolecules **47**, 4840 (2014)
7. R. Thomas, Gene **135**, 77 (1993)
8. H. Schiessel, *Biophysics for Beginners: A Journey through the Cell Nucleus* (Pan Stanford Publishing, Singapore, 2014)
9. A. Revyakin, R.H. Ebright, T.R. Strick, Proc. Natl. Acad. Sci. **101**, 4777 (2004)
10. B.P. Belotserkovskii, Phys. Rev. E **89**, 022709 (2014)
11. A.K. Dasanna, N. Destainville, J. Palmeri, M. Manghi EPL **98** 38002 (2012); *ibid* Phys. Rev. E **87**, 052703 (2013)
12. A. Baumgärtner, M. Muthukumar, J. Chem. Phys. **84**, 440 (1986)

13. M. Baiesi, R. Livi, J. Phys. A: Math. Theor. **42**, 082003 (2009)
14. R. Frederickx, T. In't Veld, E. Carlon, Phys. Rev. Lett. **112**, 198102 (2014)
15. J.C. Walter, G.T. Barkema, E. Carlon, J. Stat. Mech.: Theory and Exp. **2011**, P10020 (2011)
16. J Rudnick, Y Hu, J. Phys. A: Math. Gen., **20**, 4421 (1987)
17. C.W. Wolgemuth, T.R. Powers, R.E. Goldstein, Phys Rev Lett **84**, 1623 (2000)
18. H. Wada, R.R. Netz, Europhys. Lett. **75**, 645 (2006)
19. H. Wada, R.R. Netz, Europhys. Lett. **87**, 38001 (2009)
20. F. Brochard-Wyart, Europhys. Lett. **23**, 105 (1993)
21. F. Brochard-Wyart, H. Hervet, P. Pincus, Europhys. Lett. **511**, 511 (1994)
22. F. Brochard-Wyart, Europhys. Lett. **30**, 387 (1995)
23. T. Sakaue, T. Saito, H. Wada, Phys. Rev. E **86**, 011804 (2012)
24. P. Rowghanian, A.Y. Grosberg, Phys. Rev. E **86**, 011803 (2012)
25. B. Obermayer, O. Hallatschek, E. Frey, K. Kroy, Eur Phys J E **23**, 375 (2007)
26. P.G. de Gennes, *Scaling Concepts in Polymer Physics* (Cornell University Press: Ithaca, USA, 1979)
27. J.A. Schellman, Biopolymers **13**, 217 (1974)
28. E. Vanden-Eijnden, G. Cicotti, Chem. Phys. Lett. **429**, 310 (2006)
29. T. Sakaue, Phys. Rev. E **81**, 041808 (2010)